Vehicle sideslip angle estimation for a heavy-duty vehicle via Extended Kalman Filter using a Rational tyre model

DI BIASE, Feliciano, LENZO, Basilio <http://orcid.org/0000-0002-8520-7953> and TIMPONE, Francesco

Citation:

Vehicle Sideslip Angle Estimation for a Heavy-Duty Vehicle via Extended Kalman Filter Using a Rational Tyre Model

FELICIANO DI BIASE[1,2], BASILIO LENZO[1], (Member, IEEE), AND FRANCESCO TIMPONE[2]

[1]Department of Engineering and Mathematics, Sheffield Hallam University, Sheffield S1 1WB, U.K.
[2]Department of Industrial Engineering, University of Naples Federico II, 80125 Napoli, Italy

Corresponding author: Basilio Lenzo (basilio.lenzo@shu.ac.uk)

ABSTRACT Vehicle sideslip angle is a key state for lateral vehicle dynamics, but measuring it is expensive and unpractical. Still, knowledge of this state would be really valuable for vehicle control systems aimed at enhancing vehicle safety, to help to reduce worldwide fatal car accidents. This has motivated the research community to investigate techniques to estimate vehicle sideslip angle, which is still a challenging problem. One of the major issues is the need for accurate tyre model parameters, which are difficult to characterise and subject to change during vehicle operation. This paper proposes a new method for estimating vehicle sideslip angle using an Extended Kalman Filter. The main novelties are: i) the tyre behaviour is described using a Rational tyre model whose parameters are estimated and updated online to account for their variation due to e.g. tyre wear and environmental conditions affecting the tyre behaviour; ii) the proposed technique is compared with two other methods available in the literature by means of experimental tests on a heavy-duty vehicle. Results show that: i) the proposed method effectively estimates vehicle sideslip angle with an error limited to 0.5 deg in standard driving conditions, and less than 1 deg for a high-speed run; ii) the tyre parameters are successfully updated online, contributing to outclassing estimation methods based on tyre models that are either excessively simple or with non-varying parameters.

INDEX TERMS Kalman filter, sideslip angle, state estimation, rational tyre model, vehicle dynamics.

LIST OF SYMBOLS

Symbol	Unit	Quantity
A	various	Dynamic matrix
a_i	m	Vehicle semi-wheelbase
a_y	m/s^2	Lateral acceleration
B	various	Matrix used to work out Q
B_c	various	Matrix used to work out B
C_F	N/rad	Front cornering stiffness
C_R	N/rad	Rear cornering stiffness
c_k	various	Control input vector
c_{1i}	rad^2	Rational tyre model parameter
c_{2i}	N/rad	Rational tyre model parameter
F_{yi}	N	Lateral force
F_{zi}	N	Vertical load
$F_{zi,0}$	N	Nominal vertical load
f	-	Function defining the dynamics of the analysed system
H	various	Matrix relating z to x
h	-	Function defining the measurements as a function of the state
J	kg m^2	Vehicle moment of inertia about a vertical axis
K	-	Kalman gain
k	-	Time step
l	m	Vehicle wheelbase
M	kg	Vehicle mass
P	various	State covariance
P^-	various	Predicted state covariance
Q	various	Process covariance matrix
R	various	Measurement covariance matrix
r	rad/s	Yaw rate
$\dot{r}$	rad/s^2	Yaw acceleration
t_i	m	Vehicle track width
u	m/s	Longitudinal vehicle speed
u_{ij}	m/s	Corrected wheel speed
$u_{m,ij}$	m/s	Measured wheel speed
V	m/s	Vehicle speed (centre of mass)

V_i	m/s	Vehicle speed at axle i
v	various	Measurement noise
w	various	Process noise
x	various	State vector
$\hat{x}^-$	various	Predicted state vector
$\hat{x}$	various	Estimated state vector
z	various	Measurement vector
α_i	rad	Slip angle
β	rad	Vehicle sideslip angle
$\dot{\beta}$	rad/s	Sideslip angle rate
Δt	s	Discretisation time
δ	rad	Front wheel steering angle
Λ	various	Matrix used to work out Q
μ	-	Friction coefficient
$\sigma_{c_{iF}}$	various	Square root of the covariance of c_{iF}
$\sigma_{c_{iR}}$	various	Square root of the covariance of c_{iR}
σ_{C_F}	rad	Square root of the covariance of C_F
σ_{C_R}	rad	Square root of the covariance of C_R
σ_{ay}	m/s^2	Square root of the covariance of the accelerometer
σ_r	rad/s	Square root of the covariance of the gyroscope
σ_δ	rad	Square root of the covariance of the steering angle sensor

Subscripts : $i = F(Front), R(Rear); j = L(Left), R(Right)$

I. INTRODUCTION

The potential of many vehicle control systems, such as the ESC (Electronic Stability Control), could be significantly enhanced with the availability of the vehicle sideslip angle. Unfortunately such parameter can only be measured with expensive optical sensors. That has motivated researchers to investigate techniques to estimate vehicle sideslip angle.

Common techniques include model-based approaches and neural networks [1]. The former are generally preferred because they are explicitly linked to the physics of the studied phenomenon, e.g. through equations describing the vehicle dynamics. Many model-based approaches exist, including Luenberger Observers [2], Sliding Mode Observers [3], and the most commonly adopted approach, i.e. the Kalman Filter [4]. Over time, several authors have proposed numerous techniques to estimate vehicle sideslip angle via Kalman Filters and their variants, including Extended Kalman Filter (EKF), Unscented Kalman Filter (UKF), Cubature Kalman Filter (CKF), Square-Root Cubature Kalman Filter (SCKF) etc. [5]–[8]. Each technique adopts different hypotheses and assumptions on the available inputs, the measurable outputs, the tyre model, and the environmental/road conditions [9]–[11]. In some cases tyre force sensors are used to facilitate the estimation process [12], but that approach is not cost-effective for passenger cars and often tyre forces need to be estimated, too [13]. Some other studies propose kinematics-based techniques that do not need a tyre model [14], [15]. More recent studies investigate the option of particle filters, which normally are rather demanding in

terms of computational capability but can provide very good performance [16], [17].

As of yet, a general solution, that works in all conditions, does not exist. That is essentially down to the high complexity and variability of the possible driving conditions, which include e.g. the progressive wear of the tyres, their behaviour in different road conditions (e.g. dry, wet, ice), the characteristics of the road (e.g. irregularity, presence of slope and/or bank angle) etc. The biggest issue with model-based approaches is that their accuracy depends on whether they include a truly representative model of the tyre behaviour, which is very challenging. In general it is difficult to obtain tyre models and/or their parameters from, e.g., the tyre manufacturers. Even so, such values are (or should be) representative only for new tyres. So the models should somehow account for changes in the tyre behaviour. Some interesting attempts in the literature propose estimators based on linear tyre models, with the estimator computing the cornering stiffness of each axle, that is updated in real time or according to rule-based criteria [5], [18], [19]. Yet, it is well known that linear tyre models are accurate only for relatively low values of tyre slip angle. Another relevant aspect of sideslip angle estimation is that the majority of works deal with standard passenger cars. Very few works deal with other types of vehicles. For example, [20] investigates articulated heavy-duty vehicles in conditions of limit of adhesion.

This paper proposes a novel vehicle sideslip angle estimator, consisting of a simple single-stage EKF approach (differently from more complex approaches such as [22]) with the following main novelties:

- the Rational tyre model [21], [22] is adopted and its parameters are estimated and updated in real time, for a better accuracy of the estimator with respect to parameter-varying estimators based on linear tyre models and estimators based on fixed tyre parameters;

- the EKF performance is assessed on experimental data collected on a heavy-duty vehicle equipped with a sideslip angle sensor. The performance of the proposed algorithm is also compared to a similar approach using a linear tyre model (inspired to the recent paper [19]) and to a Rational model-based filter with no tyre parameter update.

An EKF is preferred over an UKF structure due to the peculiarities of the problem at hand, including the need of ease of tuning and low computational burden [23], with the perspective of real-time application of the estimator for advanced real-time controllers, aimed at enhancing vehicle safety.

The remainder of this paper is structured as follows. Section II introduces the vehicle model and the tyre models. Section III discusses the framework of the three filters. Results are presented in Section IV, and the main conclusions are in Section V.

II. VEHICLE MODEL

The dynamics of the vehicle is based on the well-known single-track vehicle model (Fig. 1) [24], [25], which assumes
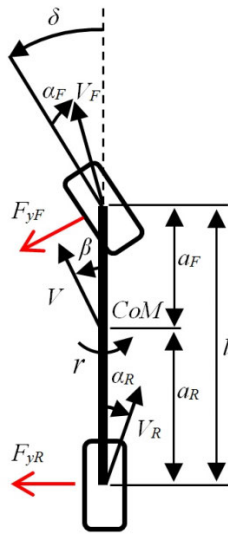
FIGURE 1. Single-track vehicle model: main parameters.

small steering angles:

$$\dot{\beta} = \frac{F_{yF}}{Mu} + \frac{F_{yR}}{Mu} - r \tag{1}$$

$$\dot{r} = \frac{F_{yF}a_F}{J} - \frac{F_{yR}a_R}{J} \tag{2}$$

The Adapted ISO sign convention [26] is used throughout the paper. Two different approaches are investigated as regards the tyre model: i) linear model; ii) Rational tyre model.

The linear tyre model is expressed as:

$$F_{yi} = C_i \alpha_i \tag{3}$$

which is a relatively good approximation only for small slip angles. The Rational model, instead, allows to capture the nonlinear behaviour of the tyre as well as its saturation. The Rational tyre model was proposed in the literature to provide a simple alternative to Pacejka's Magic Formula [21], [22], still incorporating features such as explicit dependence on normal load and road adhesion coefficient. The expression of the Rational tyre model herein adopted is ([22]):

$$F_{yi} = c_{2i}\mu \frac{F_{zi}}{F_{zi,0}} \left(\frac{\alpha_i c_{1i} (\mu + 1)}{\alpha_i^2 + c_{1i} (\mu + 1)} \right) \tag{4}$$

where c_1 and c_2 are constant parameters and μ is the tyre-road friction coefficient.

Taking into account the standard linearised congruence equations [14]:

$$\alpha_F = \delta - \left(\beta + \frac{r}{u}a_F \right) \tag{5}$$

$$\alpha_R = - \left(\beta - \frac{r}{u}a_R \right) \tag{6}$$

and using them in (3) and (4), the constitutive equations for the front and rear axles can be rewritten for the linear model as:

$$F_{yF} = C_F \left(\delta - \beta - \frac{r}{u}a_F \right) \tag{7}$$

$$F_{yR} = -C_R \left(\beta - \frac{r}{u}a_R \right) \tag{8}$$

and for the Rational tyre model as:

$$F_{yF} = c_{2F}\mu \frac{F_{zF}}{F_{zF,0}} \frac{\left(\delta - \beta - \frac{r}{u}a_F \right) c_{1F} (\mu + 1)}{\left(\delta - \beta - \frac{r}{u}a_F \right)^2 + c_{1F} (\mu + 1)} \tag{9}$$

$$F_{yR} = c_{2R}\mu \frac{F_{zR}}{F_{zR,0}} \frac{\left(-\beta + \frac{r}{u}a_R \right) c_{1R} (\mu + 1)}{\left(-\beta + \frac{r}{u}a_R \right)^2 + c_{1R} (\mu + 1)} \tag{10}$$

III. DESIGN OF THE EXTENDED KALMAN FILTER

According to the general formulation of an Extended Kalman Filter (EKF), the dynamics of the system at a generic discretisation step can be expressed by the non-linear stochastic difference equation [4]:

$$x_{k+1} = f (x_k, c_k, w_k) \tag{11}$$

where the process noise, w, is meant to account for unmodelled effects and external disturbances. w has zero mean and covariance Q. A model is also needed to relate the available measurements to the state vector:

$$z_{k+1} = h (x_{k+1}, v_{k+1}) \tag{12}$$

which accounts for sensor noise through the measurement noise vector v, that has zero mean and covariance R.

The estimation operates through the well-known prediction-correction cycle [4] expressed by an a-priori estimation (prediction):

$$\hat{x}_{k+1}^- = f(\hat{x}_k, c_k, 0) \tag{13}$$

$$P_{k+1}^- = A_k P_k A_k^T + Q \tag{14}$$

and an a-posteriori estimation (correction) based on the available measurements:

$$\hat{x}_{k+1} = \hat{x}_{k+1}^- + K_{k+1} \left(z_{k+1} - H_{k+1}\hat{x}_{k+1}^- \right) \tag{15}$$

where

$$K_{k+1} = P_{k+1}^- H_{k+1}^T \left(H_{k+1}P_{k+1}^- H_{k+1}^T + R \right)^{-1} \tag{16}$$

$$P_{k+1} = (I - K_{k+1}H_{k+1}) P_{k+1}^- \tag{17}$$

A_k is the Jacobian matrix of partial derivatives of f with respect to the state vector x:

$$A_k = \frac{\partial f}{\partial x}(\hat{x}_k, c_k, 0) \tag{18}$$

and H_{k+1} is the Jacobian matrix of partial derivatives of h with respect to x:

$$H_{k+1} = \frac{\partial h}{\partial x}(\hat{x}_{k+1}^-) \tag{19}$$

In the present case study, the control input is the front wheel steering angle, δ, and the measured quantities are the yaw rate, r, and the lateral acceleration, a_y. Both measurements are obtained through an Inertial Measurement Unit (IMU) which integrates a three-axis gyroscope and a three-axis

accelerometer. The sensor noise is reflected in the diagonal matrix R:

$$R = diag\left(\sigma_r^2, \sigma_{ay}^2\right) \qquad (20)$$

where the values of σ_r and σ_{ay} were obtained through the sensor datasheet.

The definitions of x, f, h and Q depend on the adopted tyre model and on whether the estimator is also aimed at estimating the tyre model parameters. A schematic of the EKF framework is depicted in Fig. 2.
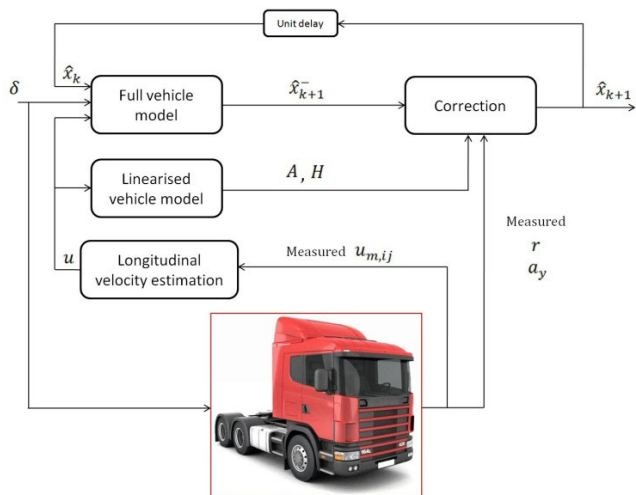

FIGURE 2. Schematic of the EKF framework.

The subsequent subsections investigate three cases: i) filter with linear tyre model and estimation of tyre parameters (LINT); ii) filter with Rational tyre model (RATT); iii) filter with Rational tyre model and estimation of tyre parameters (RATTE).

A. FILTER WITH LINEAR TYRE MODEL (LINT)
This version of the filter employs equations (7) and (8) in equations (1) and (2). Differently from conventional approaches, the values of C_F and C_R are not fixed. The state vector includes them as augmented variables, to be estimated by the filter. As discussed, the rationale is that the potentially available values of C_F and C_R might not be accurate, and that anyway they are subject to change.

The state vector is chosen as:

$$x = \left[\beta, r, \dot\beta, \dot r, C_F, C_R\right]^T \qquad (21)$$

and, by using the forward Euler method, the equations of the dynamics of the system in discrete time are:

$$\beta_{k+1} = \beta_k + \dot\beta_k \Delta t \qquad (22)$$

$$r_{k+1} = r_k + \dot r_k \Delta t \qquad (23)$$

$$\dot\beta_{k+1} = -\left(\frac{C_{F,k}+C_{R,k}}{Mu}\right)\beta_k - \left(\frac{C_{F,k}a_F - C_{R,k}a_R}{Mu^2}+1\right)r_k$$
$$+ \frac{C_{F,k}\delta_k}{Mu} \qquad (24)$$

$$\dot r_{k+1} = -\left(\frac{C_{F,k}a_F - C_{R,k}a_R}{J}\right)\beta_k$$
$$- \left(\frac{C_{F,k}a_F^2 + C_{R,k}a_R^2}{Ju}\right)r_k + \frac{C_{F,k}a_F\delta_k}{J} \qquad (25)$$

$$C_{F,k+1} = C_{F,k} \qquad (26)$$

$$C_{R,k+1} = C_{R,k} \qquad (27)$$

By studying the stability of the system defined by equations (1-3) and (5-6), it turns out that the problem is not stiff [27]. Specifically, for the case study vehicle, the ratio between the two eigenvalues of the system is 1 above 6 m/s, and up to $\sim$1.3 at low speeds. This supports the use of the forward Euler method.

Equations (26) and (27) show that no change is expected for C_F and C_R in the prediction model. The reason is that their dynamics is not known. Therefore, the variation of such parameters takes place within the correction phase of the filter.

The dynamics of the system is nonlinear - hence an EKF is used - only because of the presence of the augmented variables C_F and C_R in the state vector. Otherwise, a classical linear Kalman Filter could be used.

By applying equation (18), A_k results as:

$$A_k = \begin{bmatrix} 1 & 0 & \Delta t & 0 & 0 & 0 \\ 0 & 1 & 0 & \Delta t & 0 & 0 \\ A_{31} & A_{32} & 0 & 0 & A_{35} & A_{36} \\ A_{41} & A_{42} & 0 & 0 & A_{45} & A_{46} \\ 0 & 0 & 0 & 0 & 1 & 0 \\ 0 & 0 & 0 & 0 & 0 & 1 \end{bmatrix} \qquad (28)$$

where

$$A_{31} = -\frac{\hat C_{F,k} + \hat C_{R,k}}{Mu} \qquad (29)$$

$$A_{32} = -\left(\frac{\hat C_{F,k}a_F - \hat C_{R,k}a_R}{Mu^2}+1\right) \qquad (30)$$

$$A_{35} = \frac{\delta_k}{Mu} - \frac{\hat\beta_k}{Mu} - \frac{\hat r_k a_F}{Mu^2} \qquad (31)$$

$$A_{36} = \frac{a_R \hat r_k}{Mu^2} - \frac{\hat\beta_k}{Mu} \qquad (32)$$

$$A_{41} = -\frac{\hat C_{F,k}a_F - \hat C_{R,k}a_R}{J} \qquad (33)$$

$$A_{42} = -\frac{\hat C_{F,k}a_F^2 + \hat C_{R,k}a_R^2}{Ju} \qquad (34)$$

$$A_{45} = \frac{\delta_k a_F}{J} - \frac{\hat r_k a_F^2}{Ju} - \frac{\hat\beta_k a_F}{J} \qquad (35)$$

$$A_{46} = \frac{\hat\beta_k a_R}{J} - \frac{\hat r_k a_R^2}{Ju} \qquad (36)$$

where the symbol ($\hat{}$) represents the estimated value of a quantity, in other words:

$$\hat x_k = \left[\hat\beta_k, \hat r_k, \hat{\dot\beta}, \hat{\dot r}, \hat C_{F,k}, \hat C_{R,k}\right]^T \qquad (37)$$

The measurement vector is:

$$z = \left[r, a_y\right]^T \qquad (38)$$

Note that the measured lateral acceleration can be directly used in the filter equations because of the particular choice of variables in the state vector. This follows from:

$$a_{y,k} = u\dot{\beta}_k + ur_k \tag{39}$$

and from the fact that $\dot{\beta}$ appears in the state vector. This is inspired from [19] and is not common in the literature. In alternative approaches that include the lateral acceleration in the measurement vector, the lateral acceleration explicitly depends on the control input, i.e. the steering angle [5], [28], [29]. Based on equations (38) and (39), it results:

$$H_k = \begin{bmatrix} 0 & 1 & 0 & 0 & 0 & 0 \\ 0 & u & u & 0 & 0 & 0 \end{bmatrix} \tag{40}$$

The process noise w is assumed to be generated by uncertainties on the input (the steering angle) and the unknown dynamics of the augmented variables. So, according to [30] and by accounting for the presence of augmented variables:

$$Q = \Delta t B_k \Lambda B_k^T \tag{41}$$

where

$$\Lambda = diag\left(\sigma_\delta^2, \sigma_{C_F}^2, \sigma_{C_R}^2\right) \tag{42}$$

$$B_k = \begin{bmatrix} & & 0 & 0 \\ & & \vdots & \vdots \\ B_{c,k} & & 0 & \vdots \\ & & 1 & 0 \\ & & 0 & 1 \end{bmatrix} \tag{43}$$

$$B_{c,k} = \frac{\partial f}{\partial c}(\hat{x}_k, c_k, 0) \tag{44}$$

B_k includes the Jacobian matrix of partial derivatives of f with respect to c, evaluated at step k, denoted as $B_{c,k}$, while the subsequent columns of B_k correspond to the augmented variables C_F and C_R. Specifically:

$$B_k = \begin{bmatrix} 0 & 0 & 0 \\ 0 & 0 & 0 \\ \dfrac{C_{F,k}}{Mu} & 0 & 0 \\ \dfrac{C_{F,k}a_F}{J} & 0 & 0 \\ 0 & 1 & 0 \\ 0 & 0 & 1 \end{bmatrix} \tag{45}$$

B. FILTER WITH RATIONAL TYRE MODEL (RATT)

This version of the filter employs equations (9) and (10) in equations (1) and (2). The tyre model parameters c_1, c_2 and μ are assumed constant. The parameters c_1 and c_2 were obtained via fitting equation (4) by using the Matlab function "lsqnonlin" on an extensive amount of experimental data, with the assumption $\mu = 1$. For the purposes of fitting, the values of lateral and vertical forces for front and rear axles were obtained through the TRICK tool [31], [32]. Fig. 3 shows the results of the fitting, and Table 1 reports the obtained parameters.
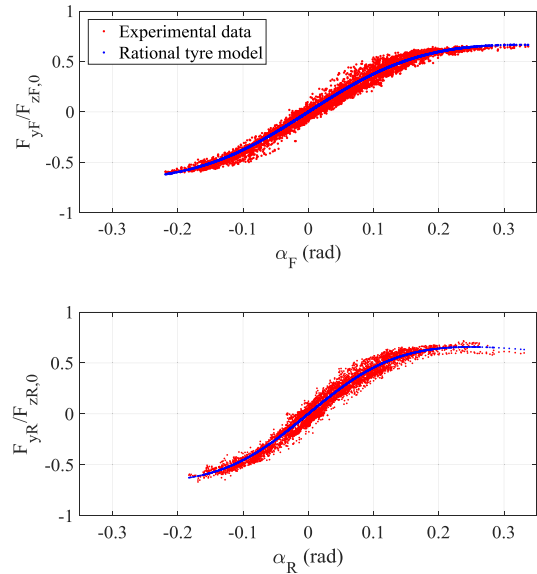
FIGURE 3. Data fitting for (top) front axle and (bottom) rear axle.

TABLE 1. Rational tyre model parameters for section III.B.

Parameter	Value and unit
c_{1F}	0.01286 rad^2
c_{2F}	486735 N/rad
c_{1R}	0.00769 rad^2
c_{2R}	622319 N/rad

Since the tyre parameters are constant, the state vector reads:

$$x = [\beta, r, \dot{\beta}, \dot{r}]^T \tag{46}$$

and the dynamics of the system is represented by four equations, i.e. equations (22) and (23) together with:

$$\dot{\beta}_{k+1} = \frac{c_{2F}\mu\frac{F_{zF}}{F_{zF,0}}\left(\frac{(\delta_k - \beta_k - \frac{r_k}{u}a_F)c_{1F}(\mu+1)}{(\delta_k - \beta_k - \frac{r_k}{u}a_F)^2 + c_{1F}(\mu+1)}\right)}{Mu}$$
$$+ \frac{c_{2R}\mu\frac{F_{zR}}{F_{zR,0}}\left(\frac{(-\beta_k + \frac{r_k}{u}a_R)c_{1R}(\mu+1)}{(-\beta_k + \frac{r_k}{u}a_R)^2 + c_{1R}(\mu+1)}\right)}{Mu} - r_k \tag{47}$$

$$\dot{r}_{k+1} = \frac{c_{2F}\mu\frac{F_{zF}}{F_{zF,0}}\left(\frac{(\delta_k - \beta_k - \frac{r_k}{u}a_F)c_{1F}(\mu+1)}{(\delta_k - \beta_k - \frac{r_k}{u}a_F)^2 + c_{1F}(\mu+1)}\right)a_F}{J}$$
$$- \frac{c_{2R}\mu\frac{F_{zR}}{F_{zR,0}}\left(\frac{(-\beta_k + \frac{r_k}{u}a_R)c_{1R}(\mu+1)}{(-\beta_k + \frac{r_k}{u}a_R)^2 + c_{1R}(\mu+1)}\right)a_R}{J} \tag{48}$$

As a result:

$$A_k = \begin{bmatrix} 1 & 0 & \Delta t & 0 \\ 0 & 1 & 0 & \Delta t \\ A_{31} & A_{32} & 0 & 0 \\ A_{41} & A_{42} & 0 & 0 \end{bmatrix} \tag{49}$$

where the expressions of each term are reported in the Appendix.

With the state vector in (46) and the same available measurements, H_k changes to:

$$H_k = \begin{bmatrix} 0 & 1 & 0 & 0 \\ 0 & u & u & 0 \end{bmatrix} \qquad (50)$$

Finally, (41) holds with:

$$\Lambda = diag\left(\sigma_\delta^2\right) \qquad (51)$$

and

$$B_k = B_{c,k} = \begin{bmatrix} 0 \\ 0 \\ B_{31} \\ B_{41} \end{bmatrix} \qquad (52)$$

where the expressions of B_{31} and B_{41} are detailed in the Appendix.

C. FILTER WITH RATIONAL TYRE MODEL AND TYRE PARAMETER ESTIMATION (RATTE)

Similarly to the previous case, this filter uses equations (9) and (10) in equations (1) and (2). However the tyre parameters c_1 and c_2 are now augmented variables in the state vector:

$$x = \left[\beta, r, \dot{\beta}, \dot{r}, c_{1F}, c_{2F}, c_{1R}, c_{2R}\right]^T \qquad (53)$$

The dynamics of the system is given by eight equations, i.e. equations (22), (23), (48), (49) and

$$c_{1F,k+1} = c_{1F,k} \qquad (54)$$

$$c_{2F,k+1} = c_{2F,k} \qquad (55)$$

$$c_{1R,k+1} = c_{1R,k} \qquad (56)$$

$$c_{2R,k+1} = c_{2R,k} \qquad (57)$$

Therefore:

$$A_k = \begin{bmatrix} 1 & 0 & \Delta t & 0 & 0 & 0 & 0 & 0 \\ 0 & 1 & 0 & \Delta t & 0 & 0 & 0 & 0 \\ A_{31} & A_{32} & 0 & 0 & A_{35} & A_{36} & A_{37} & A_{38} \\ A_{41} & A_{42} & 0 & 0 & A_{45} & A_{46} & A_{47} & A_{48} \\ 0 & 0 & 0 & 0 & 1 & 0 & 0 & 0 \\ 0 & 0 & 0 & 0 & 0 & 1 & 0 & 0 \\ 0 & 0 & 0 & 0 & 0 & 0 & 1 & 0 \\ 0 & 0 & 0 & 0 & 0 & 0 & 0 & 1 \end{bmatrix} \qquad (58)$$

Finally, (41) holds with:

$$\Lambda = diag\left(\sigma_\delta^2, \sigma_{c_{1F}}^2, \sigma_{c_{2F}}^2, \sigma_{c_{1R}}^2, \sigma_{c_{2R}}^2\right) \qquad (59)$$

and

$$B_k = \begin{bmatrix} 0 & 0 & 0 & 0 & 0 \\ 0 & 0 & 0 & 0 & 0 \\ B_{31} & 0 & 0 & 0 & 0 \\ B_{41} & 0 & 0 & 0 & 0 \\ 0 & 1 & 0 & 0 & 0 \\ 0 & 0 & 1 & 0 & 0 \\ 0 & 0 & 0 & 1 & 0 \\ 0 & 0 & 0 & 0 & 1 \end{bmatrix} \qquad (60)$$

IV. RESULTS

The performance of the three filters was assessed through experimental data obtained on the heavy-duty vehicle shown in Fig. 4. The main vehicle parameters are in Table 2. The vehicle was equipped with wheel speed sensors, a steering wheel sensor, a Racelogic Inertial Measurement Unit RLVBIMU04 V2, and a Kistler Correvit S-350 sensor. The sampling frequency was 20 Hz, resulting in a filter discretisation time step of 0.05 s. This is enough to capture the frequencies of interest in vehicle dynamics [33] while limiting the computational burden.

FIGURE 4. The instrumented vehicle used in the experimental analysis.

TABLE 2. Vehicle parameters.

Parameter	Value and unit
M	12000 kg
J	72293 kgm^2
a_F	2.25 m
a_R	2.25 m
t_F	2.32 m
t_R	2.32 m

As shown in the equations of the filters in the previous section, the longitudinal velocity, u, is needed. That is computed as a function of the measured four wheel speeds. Specifically, such values are corrected, as suggested by [14]:

$$u_{FL} = u_{FL,m} \cos(\delta) + r\left(\frac{t_F}{2}\right) \qquad (61)$$

$$u_{FR} = u_{FR,m} \cos(\delta) - r\left(\frac{t_F}{2}\right) \qquad (62)$$

$$u_{RL} = u_{RL,m} + r\left(\frac{t_R}{2}\right) \qquad (63)$$

$$u_{RR} = u_{RR,m} - r\left(\frac{t_R}{2}\right) \qquad (64)$$

and then their average is taken as the estimated longitudinal velocity.

Fig. 5 shows a sample timeframe comparing the four wheel speeds before and after correction, together with the actual longitudinal vehicle velocity, u, measured by the Kistler Correvit sensor.
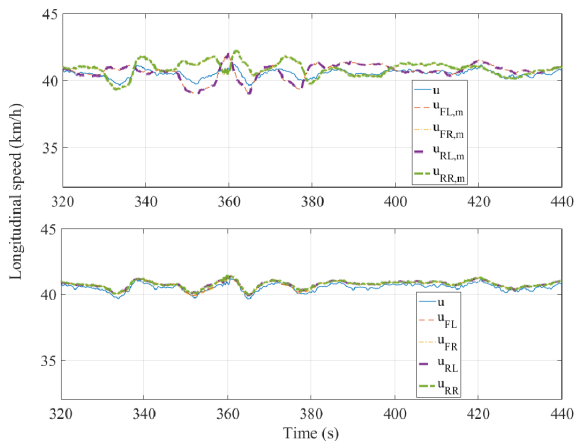

FIGURE 5. Longitudinal speed comparison: (top) measured values; (bottom) corrected values.

Fig. 6 shows the measured sideslip angle (from the Correvit sensor) along with the estimate of the filters along three consecutive laps on the Vairano track, Italy. The speed of each lap was around 30, 40 and 45 km/h respectively. The speed profile and the lateral acceleration are depicted in Figure 7, showing that lap 1 was between 0 and 299 s, lap 2 between 299 and 526 s, and lap 3 between 526 and 721 s. By multiplying each laptime and speed, the approximate track length is obtained, i.e. 2.5 km. The pattern of the lateral acceleration profile is the same for the three laps, with a few positive and negative peaks at the beginning of the lap due to the handling section (highlighted in green in Fig. 6a), then another important peak at the hairpin bend before the main straight. The magnitude of the acceleration peaks increases as the lap speed increases.

By looking at Fig. 6b, the RATTE filter produces a good estimate of the sideslip angle all round, performing much better than LINT and RATT. Interestingly, the filter performance improves with the vehicle speed. In straight driving conditions the performance of LINT, RATT and RATTE is rather similar, as shown in Fig. 6c which refers to the straight highlighted in red in Fig. 6a. On the other hand, the RATTE filter is significantly better in cornering conditions - which is when sideslip angle matters the most - as shown in Fig. 6d, which refers to the handling section highlighted in green in Fig. 6a. In particular, Fig. 6b clearly shows that LINT and RATT tend to underestimate the vehicle sideslip angle, which is an important drawback from the safety point of view. In fact, potential safety-critical condition are normally associated to relatively large values of sideslip angle [34], hence the need to promptly detect such instances, which the RATTE filter proved able to do. It is also important to note that at the
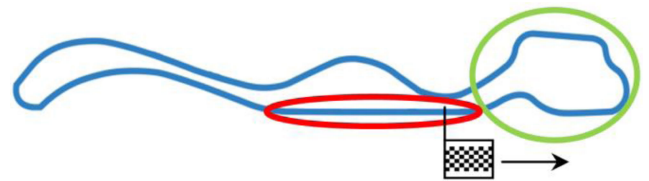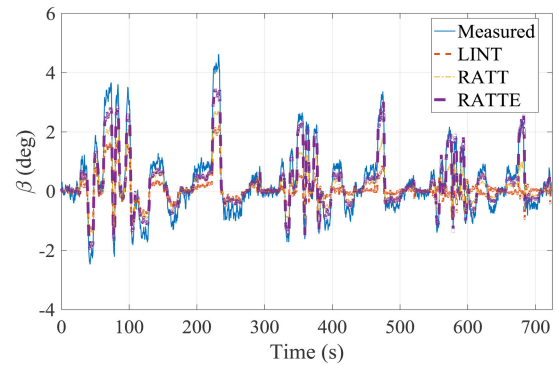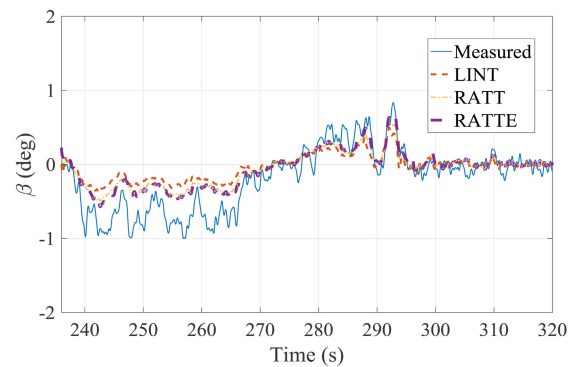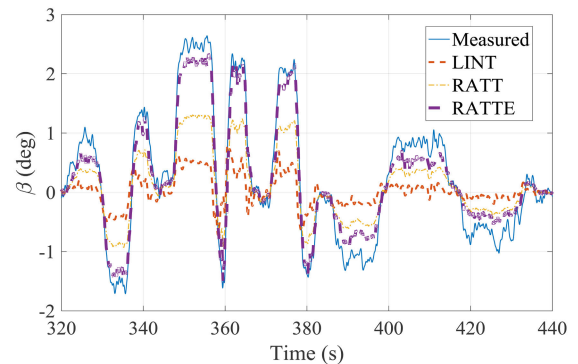

FIGURE 6. (a) Vairano track, highlight of the start/finish point, a straight (red) and a handling section (green); (b) Measured and estimated β; (c) Detail of the filter performance on the highlighted straight; (d) Detail of the filter performance on the highlighted handling section.

end of the three laps the vehicle decelerated from 45 km/h to zero speed in around 5 seconds, and the performance of the three filters remained satisfactory until ~0.4 seconds before
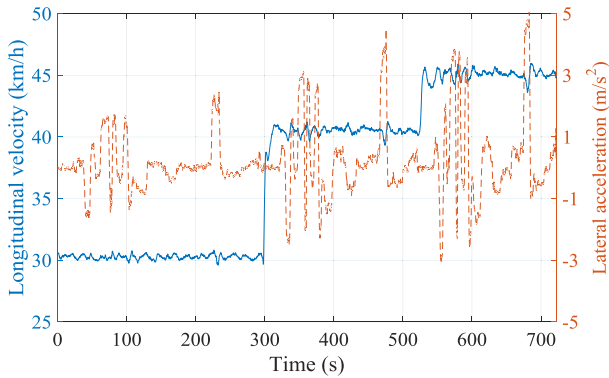
FIGURE 7. Vehicle speed and lateral acceleration during three constant speed laps.

FIGURE 8. Cornering stiffness values, LINT filter.

stopping, when also the measured value started to diverge due to the optical nature of the sensor.

To assess the performance of each filter, the sideslip angle Root Mean Square Error (RMSE) was introduced:

$$RMSE = \sqrt{\frac{\sum_{k=1}^{N}\left(\hat{\beta}_k - \beta_k\right)^2}{N}} \qquad (65)$$

in which $\hat{\beta}_k$ is the estimated value of the sideslip angle and β_k is the value of the measured sideslip angle, at time step k. N is the number of samples. The RMSE values of the three filters are reported in Table 3, which confirms that the RATTE filter outperforms the other two. By comparing RATT and LINT, the former presents a 37% improvement with respect to latter. By allowing the tyre parameters to change, RATTE improves RATT by 44%, with an overall 65% improvement with respect to LINT. In terms of absolute values the performance of RATTE is deemed satisfactory, with an error smaller than 0.5 deg.

TABLE 3. Performance analysis, constant speed laps.

Filter	RMSE (deg)
Linear tyre model (LINT)	0.8226
Rational tyre model (RATT)	0.5221
Rational tyre model, with estimation of tyre parameters (RATTE)	0.2898

The time histories of the estimated tyre parameters are shown in Fig. 8 (LINT) and Fig. 9 (RATTE). As expected their variation is relatively limited, yet significant for the filter performance.

The performance of the developed filters was also assessed on a high speed lap with a top speed of 115 km/h and average speed 76 km/h. As depicted in Fig. 10, the RATTE filter still works well and outperforms the other two. Its RMSE value is 0.62 deg, a bit larger than for the constant speed laps due
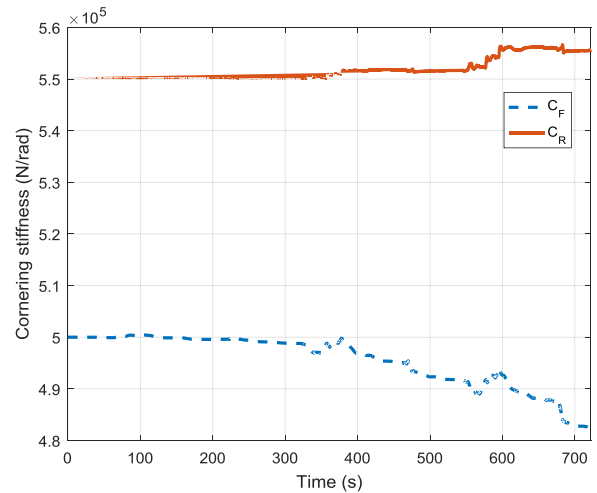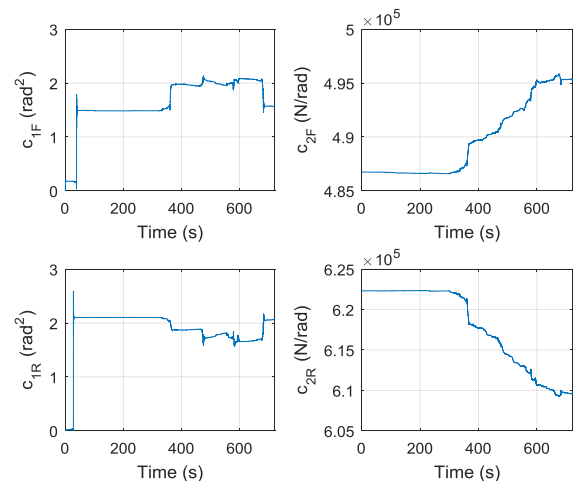

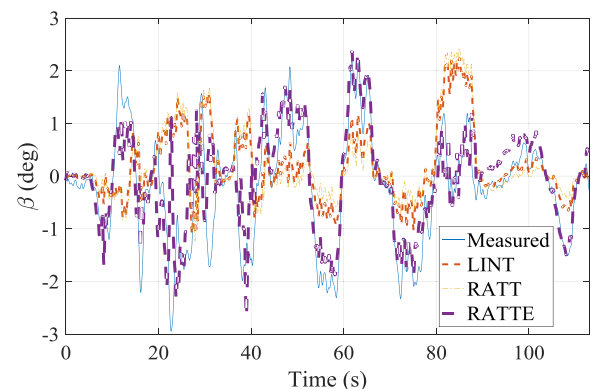**FIGURE 9.** Rational tyre model parameters, RATTE filter.

FIGURE 10. Measured and estimated β during a high speed lap.

to the more challenging manoeuvre (see speed and lateral acceleration profiles in Fig. 11), but still satisfactory in terms of sideslip angle tracking. Both LINT and RATT resulted less accurate, with RMSE values slightly above 1 deg.
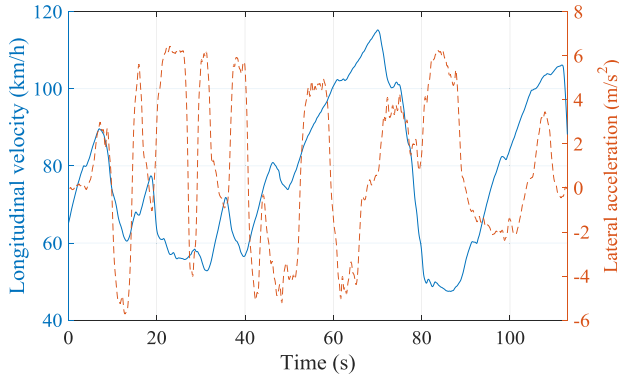
FIGURE 11. Vehicle speed and lateral acceleration during a high speed lap.

V. CONCLUSION

This paper presented an EKF approach to the estimation of the vehicle sideslip angle. After analysing a linear tyre model approach inspired to a recent approach proposed in the literature, an EKF framework was developed based on the Rational tyre model. A further evolution of the algorithm was also conceived, allowing the possibility for the filter to estimate relevant tyre parameters. The experimental results confirmed the effectiveness of the proposed approach, providing significant benefits with respect to the linear approach, with a limited increase in complexity.

Future developments include: i) the development of a more detailed vehicle model, including effects such as road slope, bank angle, vehicle roll and pitch motions; ii) the investigation of further alternative tyre models; iii) the implementation of a more advanced estimation algorithm, bearing in mind the need for low computational cost; and iv) the real-time implementation of the filter on the vehicle (e.g. through a dSPACE board) and the execution of further experimental tests, including scenarios with variable friction conditions (e.g. dry-wet).

APPENDIX

The terms in equations (49) are:

$$A_{31} = \frac{2F_{zF}\mu c_{1F}c_{2F}(\mu+1)\left(-\delta_k+\hat{\beta}_k+\frac{\hat{r}_k}{u}a_F\right)^2}{F_{zF,0}Mu\left(\left(-\delta_k+\hat{\beta}_k+\frac{\hat{r}_k}{u}a_F\right)^2+c_{1F}(\mu+1)\right)^2}$$
$$-\frac{F_{z1}\mu c_{1F}c_{2F}(\mu+1)}{F_{zF,0}Mu\left(\left(-\delta_k+\hat{\beta}_k+\frac{\hat{r}_k}{u}a_F\right)^2+c_{1F}(\mu+1)\right)}$$
$$+\frac{2F_{zR}\mu c_{1R}c_{2R}(\mu+1)\left(\hat{\beta}_k-\frac{\hat{r}_k}{u}a_R\right)^2}{F_{zR,0}Mu\left(\left(\hat{\beta}_k-\frac{\hat{r}_k}{u}a_R\right)^2+c_{1R}(\mu+1)\right)^2}$$
$$-\frac{F_{zR}\mu c_{1R}c_{2R}(\mu+1)}{F_{zR,0}Mu\left(\left(\hat{\beta}_k-\frac{\hat{r}_k}{u}a_R\right)^2+c_{1R}(\mu+1)\right)}$$

$$A_{32} = \frac{2F_{zF}\mu a_F c_{1F}c_{2F}(\mu+1)\left(-\delta_k+\hat{\beta}_k+\frac{\hat{r}_k}{u}a_F\right)^2}{F_{zF,0}Mu^2\left(\left(-\delta_k+\hat{\beta}_k+\frac{\hat{r}_k}{u}a_F\right)^2+c_{1F}(\mu+1)\right)^2}$$
$$-\frac{F_{zF}\mu a_F c_{1F}c_{2F}(\mu+1)}{F_{zF,0}Mu^2\left(\left(-\delta_k+\hat{\beta}_k+\frac{\hat{r}_k}{u}a_F\right)^2+c_{1F}(\mu+1)\right)}$$
$$-\frac{2F_{zR}\mu a_R c_{1R}c_{2R}(\mu+1)\left(\hat{\beta}_k-\frac{\hat{r}_k}{u}a_R\right)^2}{F_{zR,0}Mu^2\left(\left(\hat{\beta}_k-\frac{\hat{r}_k}{u}a_R\right)^2+c_{1R}(\mu+1)\right)^2}$$
$$+\frac{F_{z2}\mu a_2 c_{1R}c_{2R}(\mu+1)}{F_{zR,0}Mu^2\left(\left(\hat{\beta}_k-\frac{\hat{r}_k}{u}a_R\right)^2+c_{1R}(\mu+1)\right)}-1$$

$$A_{41} = \frac{2F_{zF}\mu a_F c_{1F}c_{2F}(\mu+1)\left(-\delta_k+\hat{\beta}_k+\frac{\hat{r}_k}{u}a_F\right)^2}{F_{zF,0}J\left(\left(-\delta_k+\hat{\beta}_k+\frac{\hat{r}_k}{u}a_F\right)^2+c_{1F}(\mu+1)\right)^2}$$
$$-\frac{F_{zF}\mu a_F c_{1F}c_{2F}(\mu+1)}{F_{zF,0}J\left(\left(-\delta_k+\hat{\beta}_k+\frac{\hat{r}_k}{u}a_F\right)^2+c_{1F}(\mu+1)\right)}$$
$$-\frac{2F_{zR}\mu a_R c_{1R}c_{2R}(\mu+1)\left(\hat{\beta}_k-\frac{\hat{r}_k}{u}a_R\right)^2}{F_{zR,0}J\left(\left(\hat{\beta}_k-\frac{\hat{r}_k}{u}a_R\right)^2+c_{1R}(\mu+1)\right)^2}$$
$$+\frac{F_{zR}\mu a_R c_{1R}c_{2R}(\mu+1)}{F_{zR,0}J\left(\left(\hat{\beta}_k-\frac{\hat{r}_k}{u}a_R\right)^2+c_{1R}(\mu+1)\right)}$$

$$A_{42} = \frac{2F_{zF}\mu a_F^2 c_{1F}c_{2F}(\mu+1)\left(-\delta_k+\hat{\beta}_k+\frac{\hat{r}_k}{u}a_F\right)^2}{F_{zF,0}Ju\left(\left(-\delta_k+\hat{\beta}_k+\frac{\hat{r}_k}{u}a_F\right)^2+c_{1F}(\mu+1)\right)^2}$$
$$-\frac{F_{zF}\mu a_F^2 c_{1F}c_{2F}(\mu+1)}{F_{zF,0}Ju\left(\left(-\delta_k+\hat{\beta}_k+\frac{\hat{r}_k}{u}a_F\right)^2+c_{1F}(\mu+1)\right)}$$
$$+\frac{2F_{zR}\mu a_R^2 c_{1R}c_{2R}(\mu+1)\left(\hat{\beta}_k-\frac{\hat{r}_k}{u}a_R\right)^2}{F_{zR,0}Ju\left(\left(\hat{\beta}_k-\frac{\hat{r}_k}{u}a_R\right)^2+c_{1R}(\mu+1)\right)^2}$$
$$\frac{F_{zR}\mu a_R^2 c_{1R}c_{2R}(\mu+1)}{F_{zR,0}Ju\left(\left(\hat{\beta}_k-\frac{\hat{r}_k}{u}a_R\right)^2+c_{1R}(\mu+1)\right)}$$

The terms in equations (58) include the expressions given above for $A_{31}, A_{32}, A_{41}, A_{42}$ (with $\hat{c}_{1F,k}, \hat{c}_{2F,k}, \hat{c}_{1Rk}, \hat{c}_{2R,k}$ instead of, respectively, $c_{1F}, c_{2F}, c_{1R}, c_{2R}$) and:

$$A_{35} = \frac{F_{zF}\mu\hat{c}_{1F,k}\hat{c}_{2F,k}(\mu+1)^2\left(-\delta_k+\hat{\beta}_k+\frac{\hat{r}_k}{u}a_F\right)}{F_{zF,0}Mu\left(\left(-\delta_k+\hat{\beta}_k+\frac{\hat{r}_k}{u}a_F\right)^2+\hat{c}_{1F,k}(\mu+1)\right)^2}$$

$$A_{36} = -\frac{F_{zF}\mu\hat{c}_{2F,k}(\mu+1)\left(-\delta_k+\hat{\beta}_k+\frac{\hat{r}_k}{u}a_F\right)}{F_{zR,0}Mu\left(\left(-\delta_k+\hat{\beta}_k+\frac{\hat{r}_k}{u}a_F\right)^2+\hat{c}_{1F,k}(\mu+1)\right)}$$

$$-\frac{F_{zF}\mu\hat{c}_{1F,k}(\mu+1)\left(-\delta_k+\hat{\beta}_k+\frac{\hat{r}_k}{u}a_F\right)}{F_{zF,0}Mu\left(\left(-\delta_k+\hat{\beta}_k+\frac{\hat{r}_k}{u}a_F\right)^2+\hat{c}_{1F,k}(\mu+1)\right)}$$

$$A_{37} = \frac{F_{zR}\mu\hat{c}_{1R,k}\hat{c}_{2R,k}(\mu+1)^2\left(\hat{\beta}_k-\frac{\hat{r}_k}{u}a_R\right)}{F_{zR,0}Mu\left(\left(\hat{\beta}_k-\frac{\hat{r}_k}{u}a_R\right)^2+\hat{c}_{1R,k}(\mu+1)\right)^2}$$

$$-\frac{F_{zR}\mu\hat{c}_{2R,k}(\mu+1)\left(\hat{\beta}_k-\frac{\hat{r}_k}{u}a_R\right)}{F_{zR,0}Mu\left(\left(\hat{\beta}_k-\frac{\hat{r}_k}{u}a_R\right)^2+\hat{c}_{1R,k}(\mu+1)\right)}$$

$$A_{38} = -\frac{F_{zR}\mu\hat{c}_{1R,k}(\mu+1)\left(\hat{\beta}_k-\frac{\hat{r}_k}{u}a_R\right)}{F_{zR,0}Mu\left(\left(\hat{\beta}_k-\frac{\hat{r}_k}{u}a_R\right)^2+\hat{c}_{1R,k}(\mu+1)\right)}$$

$$A_{45} = \frac{F_{zF}\mu a_F\hat{c}_{1F,k}\hat{c}_{2F,k}(\mu+1)^2\left(-\delta_k+\hat{\beta}_k+\frac{\hat{r}_k}{u}a_F\right)}{F_{zF,0}J\left(\left(-\delta_k+\hat{\beta}_k+\frac{\hat{r}_k}{u}a_F\right)^2+\hat{c}_{1F,k}(\mu+1)\right)^2}$$

$$-\frac{F_{zF}\mu a_F\hat{c}_{2F,k}(\mu+1)\left(-\delta_k+\hat{\beta}_k+\frac{\hat{r}_k}{u}a_F\right)}{F_{zF,0}J\left(\left(-\delta_k+\hat{\beta}_k+\frac{\hat{r}_k}{u}a_F\right)^2+\hat{c}_{1F,k}(\mu+1)\right)}$$

$$A_{46} = -\frac{F_{zF}\mu a_F\hat{c}_{1F,k}(\mu+1)\left(-\delta_k+\hat{\beta}_k+\frac{\hat{r}_k}{u}a_F\right)}{F_{zF,0}J\left(\left(-\delta_k+\hat{\beta}_k+\frac{\hat{r}_k}{u}a_F\right)^2+\hat{c}_{1F,k}(\mu+1)\right)}$$

$$A_{47} = -\frac{F_{zR}\mu a_R\hat{c}_{1R,k}\hat{c}_{2R,k}(\mu+1)^2\left(\hat{\beta}_k-\frac{\hat{r}_k}{u}a_R\right)}{F_{zR,0}J\left(\left(\hat{\beta}_k-\frac{\hat{r}_k}{u}a_R\right)^2+\hat{c}_{1R,k}(\mu+1)\right)^2}$$

$$+\frac{F_{zR}\mu a_R\hat{c}_{2R,k}(\mu+1)\left(\hat{\beta}_k-\frac{\hat{r}_k}{u}a_R\right)}{F_{zR,0}J\left(\left(\hat{\beta}_k-\frac{\hat{r}_k}{u}a_R\right)^2+\hat{c}_{1R,k}(\mu+1)\right)}$$

$$A_{48} = \frac{F_{zR}\mu a_R\hat{c}_{1R,k}(\mu+1)\left(\hat{\beta}_k-\frac{\hat{r}_k}{u}a_R\right)}{F_{zR,0}J\left(\left(\hat{\beta}_k-\frac{\hat{r}_k}{u}a_R\right)^2+\hat{c}_{1R,k}(\mu+1)\right)}$$

The terms in equation (52) are:

$$B_{31} = -\frac{2F_{zF}\mu c_{1F}c_{2F}(\mu+1)\left(-\delta_k+\hat{\beta}_k+\frac{\hat{r}_k}{u}a_F\right)^2}{F_{zF,0}Mu\left(\left(-\delta_k+\hat{\beta}_k+\frac{\hat{r}_k}{u}a_F\right)^2+c_{1F}(\mu+1)\right)^2}$$

$$+\frac{F_{zF}\mu c_{1F}c_{2F}(\mu+1)}{F_{zF,0}Mu\left(\left(-\delta_k+\hat{\beta}_k+\frac{\hat{r}_k}{u}a_F\right)^2+c_{1F}(\mu+1)\right)}$$

$$B_{41} = -\frac{2F_{z1}\mu a_F c_{1F}c_{2F}(\mu+1)\left(-\delta_k+\hat{\beta}_k+\frac{\hat{r}_k}{u}a_F\right)^2}{F_{zF,0}J\left(\left(-\delta_k+\hat{\beta}_k+\frac{\hat{r}_k}{u}a_F\right)^2+c_{1F}(\mu+1)\right)^2}$$

$$+\frac{F_{zF}\mu a_F c_{1F}c_{2F}(\mu+1)}{F_{zF,0}J\left(\left(-\delta_k+\hat{\beta}_k+\frac{\hat{r}_k}{u}a_F\right)^2+c_{1F}(\mu+1)\right)}$$

The terms in equation (60) include the expressions given above for B_{31} and B_{32}, using $\hat{c}_{1F,k}$, $\hat{c}_{2F,k}$, $\hat{c}_{1Rk}$, $\hat{c}_{2R,k}$ instead of, respectively, c_{1F}, c_{2F}, c_{1R}, c_{2R}.

REFERENCES

[1] D. Chindamo, B. Lenzo, and M. Gadola, "On the vehicle sideslip angle estimation: A literature review of methods, models, and innovations," *Appl. Sci.*, vol. 8, no. 3, p. 355, Mar. 2018.

[2] N. Ding, W. Chen, Y. Zhang, G. Xu, and F. Gao, "An extended Luenberger observer for estimation of vehicle sideslip angle and road friction," *Int. J. Vehicle Des.*, vol. 66, no. 4, pp. 385–414, 2014.

[3] S. Cheng, L. Li, B. Yan, C. Liu, X. Wang, and J. Fang, "Simultaneous estimation of tire side-slip angle and lateral tire force for vehicle lateral stability control," *Mech. Syst. Signal Process.*, vol. 132, pp. 168–182, Oct. 2019.

[4] G. Welch and G. Bishop, "An introduction to the Kalman Filter," in *Proc. SIGGRAPH*, 2006, pp. 1–16.

[5] F. Cheli, E. Sabbioni, M. Pesce, and S. Melzi, "A methodology for vehicle sideslip angle identification: Comparison with experimental data," *Vehicle Syst. Dyn.*, vol. 45, no. 6, pp. 549–563, Jun. 2007.

[6] B.-C. Chen and F.-C. Hsieh, "Sideslip angle estimation using extended Kalman filter," *Vehicle Syst. Dyn.*, vol. 46, no. sup1, pp. 353–364, Sep. 2008.

[7] B. L. Boada, M. J. L. Boada, and V. Diaz, "Vehicle sideslip angle measurement based on sensor data fusion using an integrated ANFIS and an unscented Kalman filter algorithm," *Mech. Syst. Signal Process.*, vols. 72–73, pp. 832–845, May 2016.

[8] S. Cheng, L. Li, and J. Chen, "Fusion algorithm design based on adaptive SCKF and integral correction for side-slip angle observation," *IEEE Trans. Ind. Electron.*, vol. 65, no. 7, pp. 5754–5763, Jul. 2018.

[9] M. Gadola, D. Chindamo, M. Romano, and F. Padula, "Development and validation of a Kalman filter-based model for vehicle slip angle estimation," *Vehicle Syst. Dyn.*, vol. 52, no. 1, pp. 68–84, Jan. 2014.

[10] C. Pieralice, B. Lenzo, F. Bucchi, and M. Gabiccini, "Vehicle sideslip angle estimation using Kalman filters: Modelling and validation," in *Proc. Int. Conf. IFToMM ITALY*. Cham, Switzerland: Springer, 2018, pp. 114–122.

[11] E. Joa, K. Yi, and Y. Hyun, "Estimation of the tire slip angle under various road conditions without tire–road information for vehicle stability control," *Control Eng. Pract.*, vol. 86, pp. 129–143, May 2019.

[12] K. Nam, S. Oh, H. Fujimoto, and Y. Hori, "Estimation of sideslip and roll angles of electric vehicles using lateral tire force sensors through RLS and Kalman filter approaches," *IEEE Trans. Ind. Electron.*, vol. 60, no. 3, pp. 988–1000, Mar. 2013.

[13] J. Dakhlallah, S. Glaser, S. Mammar, and Y. Sebsadji, "Tire-road forces estimation using extended Kalman filter and sideslip angle evaluation," in *Proc. Amer. Control Conf.*, Jun. 2008, pp. 4597–4602.

[14] D. Selmanaj, M. Corno, G. Panzani, and S. M. Savaresi, "Vehicle sideslip estimation: A kinematic based approach," *Control Eng. Pract.*, vol. 67, pp. 1–12, Oct. 2017.

[15] A. Y. Ungoren, H. Peng, and H. E. Tseng, "A study on lateral speed estimation methods," *Int. J. Vehicle Auton. Syst.*, vol. 2, nos. 1–2, pp. 126–144, 2004.

[16] K. György, A. Kelemen, and L. Dávid, "Unscented Kalman filters and particle filter methods for nonlinear state estimation," *Procedia Technol.*, vol. 12, pp. 65–74, Jan. 2014.

[17] B. Lenzo and R. De Castro, "Vehicle sideslip estimation for four-wheel-steering vehicles using a particle filter," in *Advances in Dynamics of Vehicles on Roads and Tracks* (Lecture Notes in Mechanical Engineering). Cham, Switzerland: Springer, 2020, pp. 1624–1634.

[18] S. van Aalst, F. Naets., B. Boulkroune, W. D. Nijs, and W. Desmet, "An adaptive vehicle sideslip estimator for reliable estimation in low and high excitation driving," *IFAC-PapersOnLine*, vol. 51, no. 9, pp. 243–248, 2018.

[19] G. Reina and A. Messina, "Vehicle dynamics estimation via augmented extended Kalman filtering," *Measurement*, vol. 133, pp. 383–395, Feb. 2019.

[20] G. Morrison and D. Cebon, "Sideslip estimation for articulated heavy vehicles at the limits of adhesion*," *Vehicle Syst. Dyn.*, vol. 54, no. 11, pp. 1601–1628, Nov. 2016.

[21] S. C. Başlamışlı and S. Solmaz, "Construction of a rational tire model for high fidelity vehicle dynamics simulation under extreme driving and environmental conditions," in *Proc. ASME 10th Biennial Conf. Eng. Syst. Design Anal.*, vol. 3, Jan. 2010, pp. 131–137.

[22] A. H. Ahangarnejad and S. Ç. Başlamışlı, "Adap-tyre: DEKF filtering for vehicle state estimation based on tyre parameter adaptation," *Int. J. Vehicle Des.*, vol. 71, nos. 1–4, pp. 52–74, 2016.

[23] M. Rhudy and Y. Gu, "Understanding nonlinear Kalman filters—Part 1: Selection of EKF or UKF," *Interact. Robot. Lett.*, Jun. 2013. [Online]. Available: https://yugu.faculty.wvu.edu/research/interactive-robotics-letters/understanding-nonlinear-kalman-filters-part-i

[24] M. Guiggiani, *The Science of Vehicle Dynamics*. Cham, Switzerland: Springer, 2018.

[25] G. Genta, *Motor Vehicle Dynamics: Modeling and Simulation*. Singapore: World Scientific Publishing, 1997.

[26] H. B. Pacejka, *Tyre and Vehicle Dynamics*. Oxford, U.K.: Butterworth-Heinemann, 2006.

[27] K. Atkinson, W. Han, and D. E. Stewart, *Numerical Solution of Ordinary Differential Equations*, vol. 108. Hoboken, NJ, USA: Wiley, 2011.

[28] F. Naets, S. van Aalst, B. Boulkroune, N. E. Ghouti, and W. Desmet, "Design and experimental validation of a stable two-stage estimator for automotive sideslip angle and tire parameters," *IEEE Trans. Veh. Technol.*, vol. 66, no. 11, pp. 9727–9742, Nov. 2017.

[29] J. Farrelly and P. Wellstead, "Estimation of vehicle lateral velocity," in *Proc. IEEE Int. Conf. Control Appl. IEEE Int. Conf. Control Appl. Held Together With IEEE Int. Symp. Intell. Control*, Sep. 1996, pp. 552–557.

[30] G. Franklin, D. Powell, and M. Workman, *Digital Control of Dynamic Systems*. Reading, MA, USA: Addison-Wesley, 1997.

[31] F. Farroni, "TRICK-Tire/Road interaction characterization & knowledge—A tool for the evaluation of tire and vehicle performances in outdoor test sessions," *Mech. Syst. Signal Process.*, vols. 72–73, pp. 808–831, May 2016.

[32] F. Farroni, G. N. Dell'Annunziata, A. Sakhnevych, F. Timpone, B. Lenzo, and M. Barbieri, "Towards T.R.I.C.K. 2.0—A tool for the evaluation of the vehicle performance through the use of an advanced sensor system," in *Proc. Conf. Italian Assoc. Theor. Appl. Mech.*, Cham, Switzerland: Springer, 2019, pp. 1093–1102.

[33] P. Perinciolo and E. Sondhi, *Model Based Handling Analyses*. Stockholm, Sweden: KTH, 2018.

[34] B. Lenzo, M. Zanchetta, A. Sorniotti, P. Gruber, and W. De Nijs, "Yaw rate and sideslip angle control through single input single output direct yaw moment control," *IEEE Trans. Control Syst. Technol.*, early access, Feb. 4, 2020, doi: 10.1109/TCST.2019.2949539.
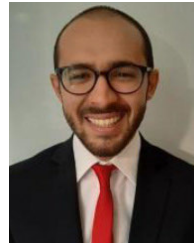
FELICIANO DI BIASE received the bachelor's degree in mechanical engineering from the Second University of Naples, Italy, in 2016, and the M.Sc. degree in mechanical engineering for design and production from the University of Naples Federico II, Italy, in 2019. He completed his internship thesis work at the Department of Engineering and Mathematics Sheffield Hallam University. His current research interests include vehicle dynamics and control.

BASILIO LENZO (Member, IEEE) received the M.Sc. degree in mechanical engineering from the University of Pisa and the University Sant'Anna, Pisa, Italy, in 2010, and the Ph.D. degree in robotics from University Sant'Anna, in 2013. In 2010, he was a Research and Development Intern with Ferrari Formula 1. Since 2016, he has been a Senior Lecturer of automotive engineering with Sheffield Hallam University. He was also a Visiting Researcher with the École Normale Supérieure Cachan, France, the University of Delaware, USA, Columbia University, USA, the University of Naples, Italy, the German Aerospace Center DLR, Germany, and the Politecnico di Torino, Italy. He was a two-time TEDx Speaker. His research interests include vehicle dynamics, state estimation, control, and robotics.

FRANCESCO TIMPONE received the M.Sc. degree in mechanical engineering and the Ph.D. degree in thermomechanical system engineering from the University of Naples Federico II, in 1999 and 2004, respectively. He is currently an Associate Professor of applied mechanics and vehicle dynamics with the University of Naples Federico II. His research interests include the dynamics and the control of mechanical systems.

• • •